Mechanics of Materials 93 (2016) 32–42

Contents lists available at ScienceDirect

Mechanics of Materials

journal homepage: www.elsevier.com/locate/mechmat

Constitutive flow behaviour and finite element simulation of hot rolling of SiCp/2009Al composite

L. Zhou [a,b], Z.Y. Huang [a], C.Z. Wang [b], X.X. Zhang [a], B.L. Xiao [a], Z.Y. Ma [a,*]

[a] Institute of Metal Research, Chinese Academy of Sciences, Shenyang 110016, China
[b] School of Mechanical Engineering, Shenyang Ligong University, Shenyang 110159, China

A R T I C L E   I N F O

Article history:
Received 1 June 2015
Revised 4 October 2015
Available online 28 October 2015

Keywords:
Composites
Constitutive modelling
Hot rolling
Finite element simulation

A B S T R A C T

The material parameters of 17vol.%SiCp/2009Al composite in the Arrhenius-type constitutive equations were calculated using experimental data from hot compression tests. The constitutive equation was then implemented into the finite element software, ABAQUS/Explicit, to calculate the stress, deformation and edge damage in the hot rolling process. The initiation and propagation of edge cracks under the hot rolling condition were studied via the Gurson–Tvergaard–Needleman (GTN) damage model. The influence of the thickness reduction on the strip damage was assessed. The results indicate that the high tensile stress at the edge of the strip causes crack initiation and propagation, and the total reduction has a significant effect on the damage in the hot rolling of the SiCp/2009Al composites. When the reduction is less than 20%, no crack initiates and the damage occurs on the strip surface. With increase of the total reduction to 25% and larger, edge cracks occur and increase gradually. The distribution and direction of edge cracks are closely correlated with the stress components. The hot rolling experiments on 17vol.%SiCp/2009Al composite were conducted to evaluate the simulation results, and it is indicated that the finite element calculation results agreed well with the experimental results. This indicates that the finite element analysis is able to successfully simulate the rolling process and provide important information for the process optimization.

1. Introduction

SiC particle reinforced Al matrix (SiCp/Al) composites have high specific strength and stiffness, high thermal conductivity, and good wear resistance compared to unreinforced matrix alloys, making them very suitable for many structural applications in the automotive and aerospace industries (Ni et al., 2013). To date, several manufacturing techniques have been developed for fabricating SiCp/Al composites, including powder metallurgy (Hassani et al., 2014), stir casting (Balasubramanian and Maheswaran, 2015) and pressureless infiltration (Liu et al., 2008), etc. Generally, with these fabrication methods, it is difficult to avoid particle clusters and porosity. Secondary processing such as rolling (El-Sabbagh et al., 2013), extrusion (Seo and Kang, 1999) and forging (Özdemir et al., 2000) is essential to decrease porosity, thereby leading to a more uniform particle distribution and improving the particle–matrix interfacial bonding.

Due to the presence of SiC particles, the stiffness and strength of the SiCp/Al composites are increased, whereas the ductility decreases significantly. Therefore, the secondary processing of SiCp/Al composites is still a big challenge, which limits their widespread application. El-Sabbagh et al. (2012) and Yan et al. (2013) have noted that edge cracking is a common problem during the rolling process, which can cause the rupture of strips and reduce the production quality. In recent years, with the increasing application of the composites, optimization of the rolling process for obtaining composites with higher quality and performance is highly desirable.

* Corresponding author. Tel./fax: +86 24 83978908.
E-mail address: zyma@imr.ac.cn (Z.Y. Ma).

http://dx.doi.org/10.1016/j.mechmat.2015.10.010
0167-6636/

It is well known that the rolling speed, rolling temperature, initial strip thickness, thickness reduction and the microstructure of composites are the main factors that determine the rolling process of the SiCp/Al composites. Pal et al. (2010) observed that cracks emerged in SiC particles and at the particle–matrix interfaces of the composites during hot rolling, and these cracks appear to increase with increasing content of SiC particles. The effect of rolling temperature on the rolling process is obvious, as demonstrated by Euh and Kang (2005) and Lu et al. (1999). At room temperature, edge cracks as well as centre cracks were shown to form even at a small thickness reduction. As the rolling temperature rises, no centre crack was achieved under the same reduction. El-Sabbagh et al. (2013) and Amirkhanlou et al. (2011) reported that as the rolling reduction ratio increased, the porosity content was reduced, and the distribution of SiC particles became more uniform. In addition, it was reported that when the size and content of SiC particles increased, the edge crack density in rolled SiCp/Al composite plates increased significantly (El-Sabbagh et al., 2012).

In addition to the experimental method, the finite element method (FEM), including both two-dimensional (Mei et al., 2010) and three-dimensional FEMs (Bagheripoor and Bisadi, 2011) has been used to simulate the rolling force, temperature field, strain distribution and the evolution of microstructure during the rolling of different metals and alloys. Yan et al. (2013) used FEM and experimental methods to analyse the initiation and propagation of cracks at the notch tip in the cold rolling process based on the Gurson–Tvergaard–Needleman (GTN) damage model. The simulated results agreed well with the experimental results (Yan et al., 2013). As yet, only limited studies have been undertaken to simulate the rolling process of the SiCp/Al composites and investigate the damage evolution using FEM.

The accuracy of the outcome of any finite element simulation depends on a good characterization of the material behaviour under working conditions (Esteban et al., 2007). Taking this into account, hot compression tests were first conducted with a wide range of strain rates and temperatures, and then the constitutive model of a 17vol.%SiCp/2009Al composite was constructed. The GTN damage model was employed to investigate the initiation and propagation of cracks near the strip edge during the rolling process under different rolling conditions by a three-dimensional thermo-mechanical FEM. The effect of the thickness reduction on the damage to the strip was detailed. Then, the hot rolling experiments of 17vol.%SiCp/2009Al composite were carried out to verify the results obtained from the finite element calculation.

2. Experimental procedures

17vol.%SiCp/2009Al composite fabricated by the powder metallurgy method and subsequent extrusion was studied in this work, as shown in Fig. 1. 2009Al alloy has a composition of Al-4.0Cu-1.4Mg (wt.%) and SiC particles have an average size of 7 μm. The detailed fabrication process has been described in a previous study (Ni et al., 2014).

In order to study the flow behaviour of the composites, uniaxial hot compression tests were conducted up to a strain of 0.69 on the Gleeble 3800 system at six different

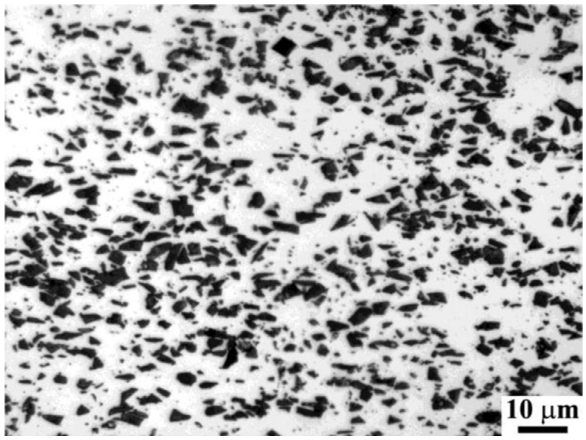

Fig. 1. Microstructure of 17vol.%SiCp/2009Al composite.

temperatures (350, 375, 400, 425, 450, 475 °C) and four strain rates (0.001, 0.01, 0.1 and 1 s^{-1}). Cylindrical specimens 8 mm in diameter and 12 mm in height were machined from the extruded rod and used for the hot compression tests.

The composite planks with dimensions of 500×145×12.5 mm^3 machined from the extruded slabs were subjected to hot rolling experiments on a rolling mill with 520 mm diameter twin rolls. Before rolling, the planks were heated at 460 °C for 60 min.

3. Constitutive equations

The true stress–true strain curves of the 17vol.% SiCp/2009Al composite at various strain rates and temperatures are plotted in Fig. 2, and were used to determine the material parameters of the Arrhenius-type constitutive equation (Sellars and McTegart, 1966). From Fig. 2, it can be observed that the influences of the temperature and strain rate on the flow stress are significant. The flow stress decreases with increasing temperature or decreasing strain rate. When the flow stress reached a steady state regime, the flow stress was no longer dependent on the strain.

According to Sellars and McTegart (1966) and Abbasi-Bani et al. (2014), the sine hyperbolic law in the Arrhenius equation with the Zener–Hollomon parameter (Z) gives a better description for flow stress calculation in all the hot working ranges. These are expressed as:

$$Z = \dot{\varepsilon} \exp\left(\frac{Q}{RT}\right). \tag{1}$$

$$\dot{\varepsilon} = AF(\sigma) \exp\left(\frac{-Q}{RT}\right) \tag{2}$$

$$F(\sigma) = \begin{cases} \sigma^{n_1} & \alpha\sigma < 0.8 \\ \exp(\beta\sigma) & \alpha\sigma > 1.2 \\ [\sinh(\alpha\sigma)]^n & for\ all\ \sigma \end{cases}. \tag{3}$$

where R is the universal gas constant (8.314 J $mol^{-1}K^{-1}$), T is the absolute temperature (K), Q is the activation energy (J mol^{-1}), A, β, n_1, α and n are experimentally determined

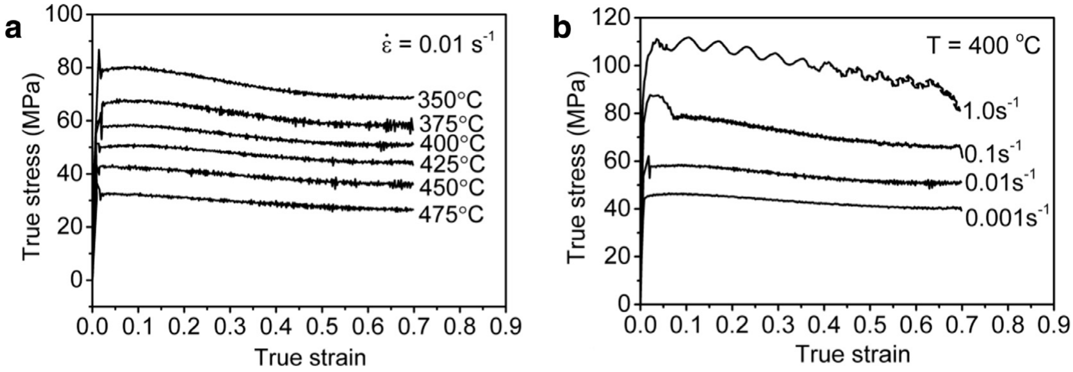

Fig. 2. True stress–strain curves of 17vol.%SiCp/2009Al composite at (a) 0.01 s^{-1} for different temperatures and (b) 400 °C for different strain rates.

temperature independent materials parameters, and $\alpha = \beta/n_1$. When the effect of temperature on the flow stress is neglected, for low and high stress levels, Eq. (2) can be simplified as Eqs. (4) and (5), respectively:

$$\dot{\varepsilon} = B\sigma^{n_1} \tag{4}$$

$$\dot{\varepsilon} = C\exp(\beta\sigma). \tag{5}$$

where B and C are the material parameters. Taking the logarithm of both sides of Eqs. (4) and (5) gives:

$$\ln\sigma = \frac{1}{n_1}\ln\dot{\varepsilon} - \frac{1}{n_1}\ln B \tag{6}$$

$$\sigma = \frac{1}{\beta}\ln\dot{\varepsilon} - \frac{1}{\beta}\ln C. \tag{7}$$

The values of n_1 and β are obtained from the slope of the linear fitting lines in the plots of $\ln\sigma$ versus $\ln\dot{\varepsilon}$ (Fig. 3a) and σ versus $\ln\dot{\varepsilon}$ (Fig. 3b), respectively. The average values of n_1 and β were calculated to be 7.58 and 0.119 MPa^{-1}, and this gives the value of $\alpha = \beta/n_1 = 0.1570$ MPa^{-1}.

For all the stress levels, Eq. (2) is rewritten as:

$$\dot{\varepsilon} = \mathrm{A}[\sinh(\alpha\sigma)]^{\mathrm{n}}\exp\left(-\frac{\mathrm{Q}}{\mathrm{RT}}\right) \tag{8}$$

Taking the logarithm of both sides of the above equation gives:

$$\ln[\sinh(\alpha\sigma)] = \frac{\ln\dot{\varepsilon}}{\mathrm{n}} + \frac{\mathrm{Q}}{\mathrm{nRT}} - \frac{\ln\mathrm{A}}{\mathrm{n}} \tag{9}$$

In the same way, the values of n and activation energy Q can be obtained from the slope of the linear fitting lines in the $\ln[\sinh(\alpha\sigma)]$versus $\ln\dot{\varepsilon}$ (Fig. 3c) and $\ln[\sinh(\alpha\sigma)]$ versus 1000/T (Fig. 3d) plots, respectively. From Fig. 3(c and d), the average values of n and Q were calculated to be 5.63 and 207 KJ/mol. It is clear that the activation energy (207 KJ/mol) is much higher than that of the lattice diffusion of aluminium (142 KJ/mol), which is because the hard SiC particles pin the motion of dislocations and grain boundaries and raise the deformation resistance (Shao et al., 2010). When the activation energy of thermal deformation is obtained, the correlation between the flow stress and deformation conditions can be described with the Z parameter in an exponent equation:

Table 1.
Calculated material parameters of the Arrhenius-type constitutive equations.

Parameter	Q (KJ/mol)	$\ln A$	n	α(MPa^{-1})
Value	206.8288	32.3723	5.4834	0.1570

$$Z = A\sinh(\alpha\sigma)^n = \dot{\varepsilon}\exp\left(\frac{Q}{RT}\right) \tag{10}$$

Taking the logarithm of both sides of Eq. (10), the material parameters A and n can be obtained from the plot of $\ln Z$versus $\ln[\sinh(\alpha\sigma)]$ (Fig. 3e), where the slope of the linear fitting line stands for the n value, and the intercept corresponds to $\ln A$. The values of n and $\ln A$ are calculated to be about 5.48 and 32.37, respectively. It should be mentioned that all material parameters above are calculated at a true strain of 0.3 and its relative coefficients are listed in Table 1.

In addition to the temperature and strain rate, the strain is another factor that affects the material parameters of the constitutive equation. Therefore, the influence of strain in the constitutive equation is incorporated by assuming that the activation energy (Q) and material parameters (n, α and $\ln A$) are the polynomial functions of strain. In the present work, the material parameters determined at strains ranging from 0.1 to 0.65 with an interval of 0.05 are fitted using a fourth-order polynomial (Eq. (11)), as shown in Fig. 4. It can be seen that the fourth-order polynomial equation captures the influence of strain on the material parameters with good accuracy.

$$\begin{aligned}
\alpha &= 0.0143 + 0.0038\varepsilon - 4.06\times10^{-4}\varepsilon^2 + 0.0213\varepsilon^3 \\
&\quad -0.0271\varepsilon^4 \\
Q &= 170.834 + 598.907\varepsilon - 2997.395\varepsilon^2 + 5815.884\varepsilon^3 \\
&\quad -3782.852\varepsilon^4 \\
n &= 4.996 + 9.546\varepsilon - 49.943\varepsilon^2 + 99.487\varepsilon^3 - 65.794\varepsilon^4 \\
\ln A &= 26.384 + 98.893\varepsilon - 491.497\varepsilon^2 + 947.261\varepsilon^3 \\
&\quad -611.686\varepsilon^4
\end{aligned} \tag{11}$$

Once the material parameters are determined, the flow stress at a particular strain can be obtained from the function of sine hyperbolic law ($\sinh^{-1}(\alpha\sigma) = \ln[\alpha\sigma + ((\alpha\sigma)^2+1)^{\frac{1}{2}}]$)

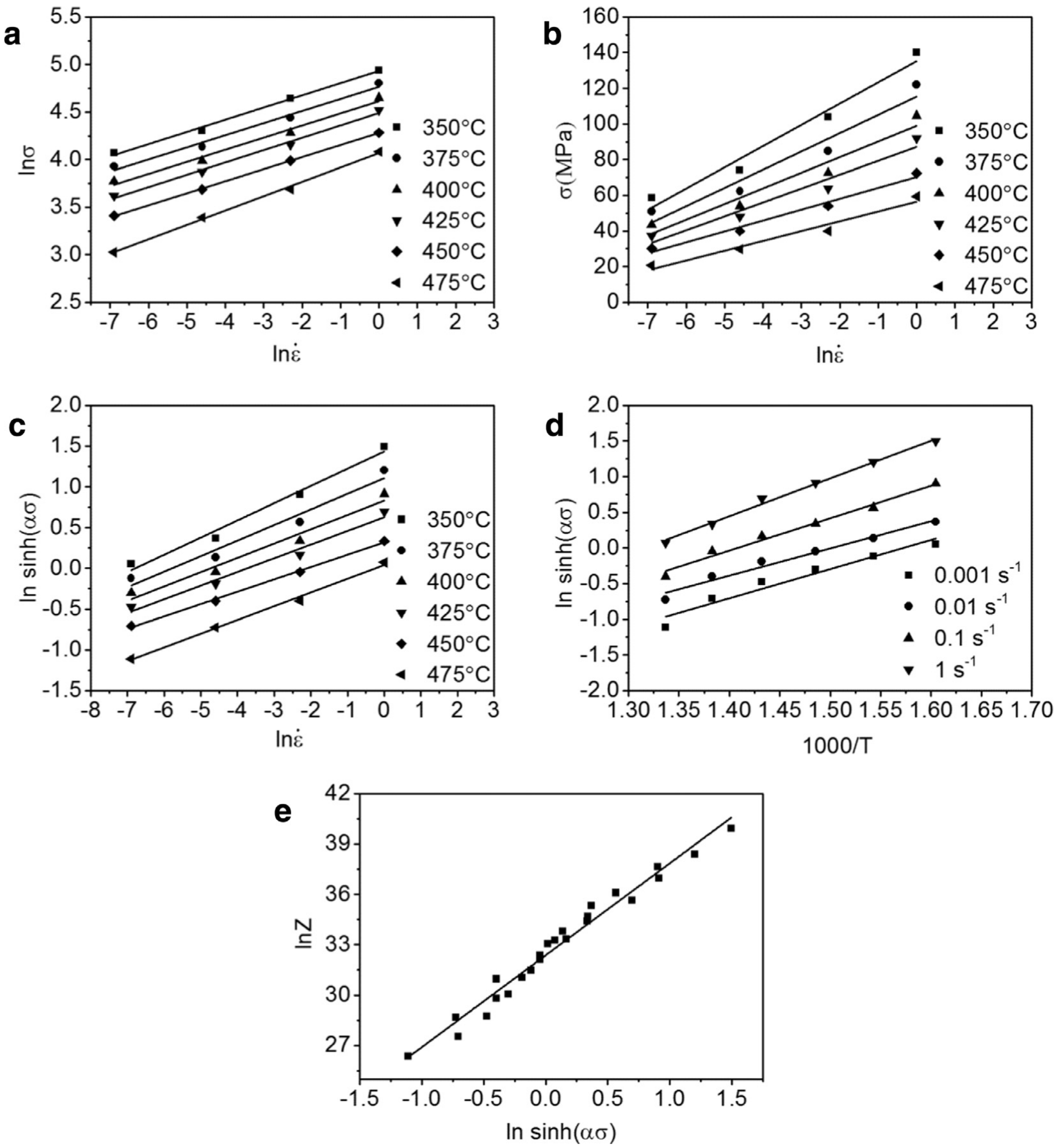

Fig. 3. Evaluation of (a) n_1 by plotting $\ln\sigma$ vs $\ln\dot{\varepsilon}$, (b) β by plotting σ vs $\ln\dot{\varepsilon}$, (c) n by plotting $\ln[\sinh(\alpha\sigma)]$ vs $\ln\dot{\varepsilon}$, (d) Q by plotting $\ln[\sinh(\alpha\sigma)]$ vs 1000/T, and (e) n and $\ln A$ by plotting $\ln Z$vs $\ln[\sinh(\alpha\sigma)]$.

and Eq. (10). Thus, the constitutive equation that relates the flow stress and Z parameter can be written as:

$$\sigma = \frac{1}{\alpha}\ln\left\{\left(\frac{Z}{A}\right)^{\frac{1}{n}} + \left[\left(\frac{Z}{A}\right)^{\frac{2}{n}} + 1\right]^{\frac{1}{2}}\right\} \tag{12}$$

Eqs. (11) and (12) are used to build the constitutive equations of the 17vol.%SiCp/2009Al composite at strain rates from 0.001 to 1.0 s^{-1} and temperatures from 350 to 475 °C, which is coded in FORTRAN in the form of a user material (VUMAT).

Fig. 5 shows the comparison between the experimental flow curves and those predicted by using the parameters summarised in Table 1 under different strain rates for six testing temperatures. It can be seen that a good correlation between experimental and predicted data is obtained, and the Arrhenius-type equation also theoretically describes the yield stress of the solid material as a function of plastic strain in the undamaged composite.

4. Rolling process simulation

4.1. Finite element model

A three-dimensional thermo-mechanical coupled simulation was carried out with the finite element software ABAQUS/Explicit. The initiation and propagation of edge cracks were studied during a single pass of the hot rolling process based on the GTN damage model. Due to the symmetry about the x–y and x–z planes, to reduce the computational time, only one quarter of the strip and half of the work roll were considered in the model, as shown in Fig. 6. The dimensions of the strip were $500\times145\times12.5$ mm^3, and the diameter of the work roll was 520 mm. The 8-node

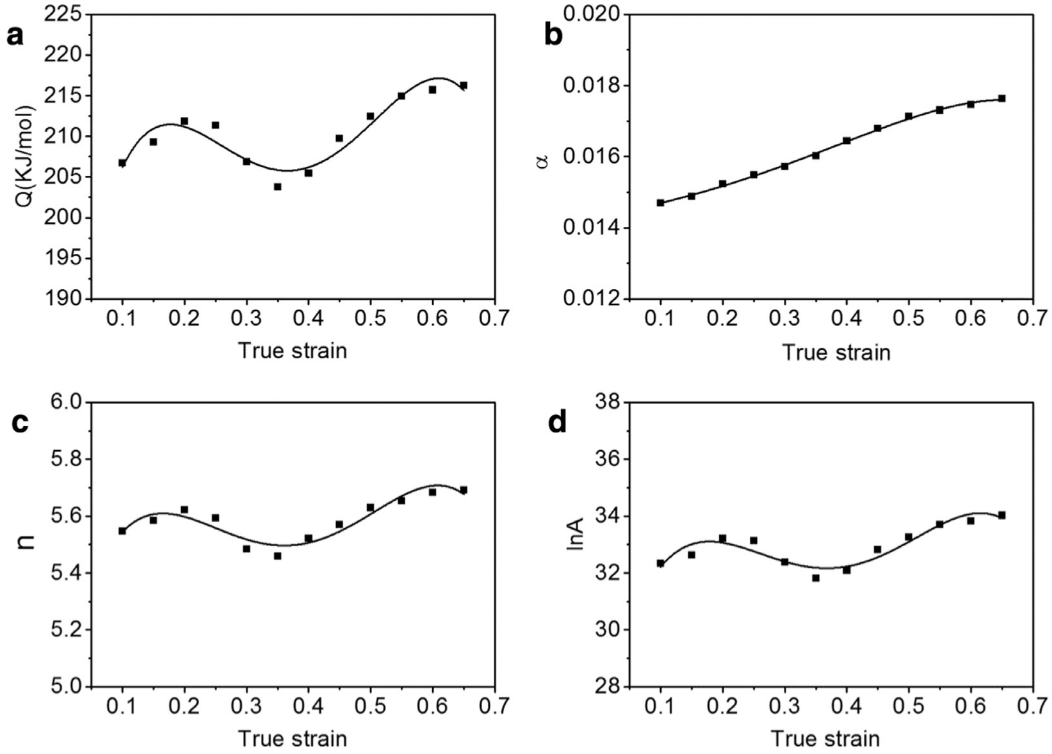

Fig. 4. Variation of (a) Q, (b) α, (c) n and (d) $\ln A$ with true strain.

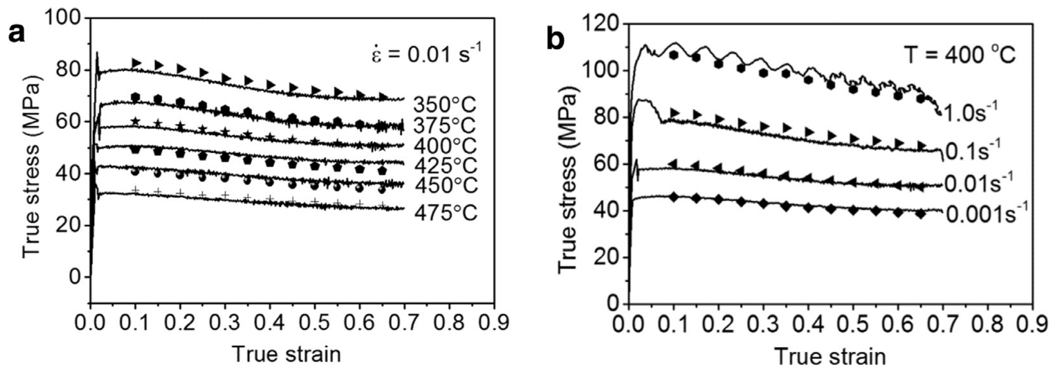

Fig. 5. Comparison between experimental and predicted flow stress (the symbols denote the predicted results and the solid lines denote the experimental data) at (a) 0.01 s^{-1} for different temperatures and (b) 400 °C for different strain rates.

trilinear displacement and temperature coupled element with reduced integration and hourglass control, C3D8RT, was employed in the finite element calculation. The global mesh size was finally designated as 1 mm which guaranteed that the meshes were convergent with respect to the overall response of the system and the detailed mesh convergence tests were discussed in our published work (Zhou et al., 2015). The work roll was assumed to be rigid and was modelled as an analytical rigid surface.

4.2. Boundary conditions and loads

In this model, both the displacement and thermal boundary conditions were defined. At the centre plane of the strip, i.e., on the x–y and x–z symmetry plane, the symmetrical displacement constraint and the adiabatic condition of temperature were imposed. The heat transfer coefficient between the strip and work roll, and the strip and air were set to 0.01 and 25 kW/(m^2·K) (Shahani et al., 2009), respectively. The initial temperature of the strip was 460 °C, and four thickness reductions, 20, 25, 30 and 40%, were studied as rolling conditions, which were named as models I, II, III and IV.

During the rolling process, one contact zone occurred between the strip surface and work roll. The contact behaviour was assumed to be controlled by the Coulomb friction law, and a constant Coulomb friction coefficient was used.

The work roll was treated as a rigid body and rotated at a tangential velocity of 0.5 m/s. To avoid rotational and translational movement of the work roll in the other directions,

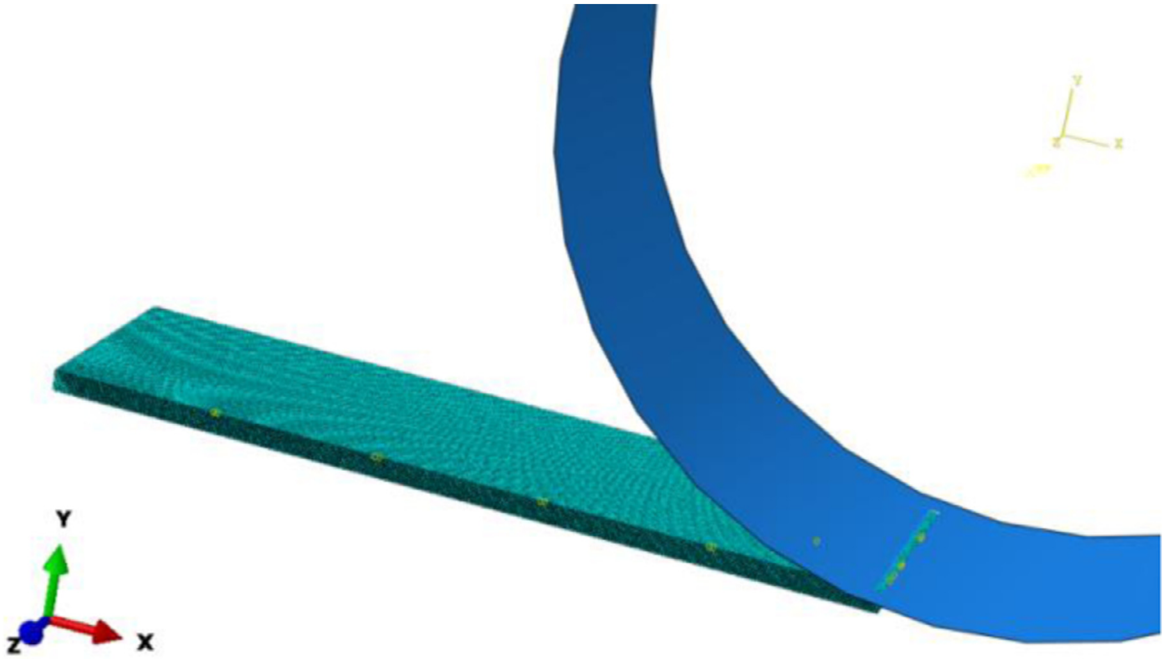

Fig. 6. Three-dimensional finite element model.

displacement constraints were set at the reference node of the work roll. Besides, to guarantee that the strip entered the rolling gap smoothly, the initial velocity for the strip was assigned to be 0.49 m/s, slightly less than the roll's tangential velocity.

4.3. Material properties and the GTN damage model

In this study, the strip was introduced as a thermo-viscoplastic material, and the Arrhenius-type constitutive equations with the determined material parameters were employed to simulate the hot rolling behaviour of the 17vol.%SiCp/2009Al composite. Due to the low content of SiC particles, the SiCp/2009Al composite was assumed to be macro-isotropic and known as the matrix or solid material even though the material contains the voids, therefore, the composite is defined as a ductile material to investigate the damage and fracture, which follows the GTN damage model. The GTN model, originally proposed by Gurson (1977) and subsequently extended by Tvergaard and Needleman (1984), is one of the most popular damage models for predicting ductile fracture. This model describes the evolution of a randomly distributed volume fraction of spherical voids in porous materials (Mansouri et al., 2014). The yield function of the GTN model is given by

$$\Phi = \left(\frac{q}{\sigma_y}\right)^2 + 2q_1 f^* \cosh\left(-q_2\frac{3p}{2\sigma_y}\right) - (1 + q_3 f^{*2}) \tag{13}$$

where σ_y is the yield stress of the fully dense matrix material as a function of the equivalent plastic strain $\bar{\varepsilon}^{pl}$, q the von Mises equivalent stress, p the hydrostatic pressure, q_1, q_2 and q_3 are the material parameters, and $f*$ is a porosity parameter depending on the void volume fraction f.

$$f^* = \begin{cases} f & if \quad f \le f_C \\ f_c + \frac{\bar{f}_F - f_C}{f_F - f_C}(f - f_C) = 0 & if \quad f_C < f < f_F \\ \bar{f}_F & if \quad f \ge f_F \end{cases} \tag{14}$$

where f_C is the critical value of the void volume fraction, and f_F the void volume fraction at final failure. The balance coefficient $\bar{f}_F$ is expressed by

$$\bar{f}_F = \frac{q_1 + \sqrt{q_1^2 - q_3}}{q_3} \tag{15}$$

The total change rate of f corresponds to the nucleation voids and the void growth

$$\dot{f} = \dot{f}_{nucl} + \dot{f}_{gr} \tag{16}$$

$$\dot{f}_{gr} = (1 - f)\dot{\varepsilon}^{pl} : I \tag{17}$$

where $\dot{f}_{gr}$ is based on the law of conservation of mass and controlled by nondeviatoric plastic strain $\dot{\varepsilon}^{pl}$, and I is the identity tensor.

$$\dot{f}_{nucl} = \frac{f_N}{s_N\sqrt{2\pi}} \exp\left[-\frac{1}{2}\left(\frac{\bar{\varepsilon}^{pl} - \varepsilon_N}{s_N}\right)^2\right]\dot{\bar{\varepsilon}}^{pl} \tag{18}$$

where $\bar{\varepsilon}^{pl}$ is the equivalent plastic strain of the matrix which control the nucleation of new voids, $\dot{\bar{\varepsilon}}^{pl}$ is the equivalent plastic strain rate. $\dot{f}_{nucl}$ is given by a strain-controlled relationship, the normal distribution of the nucleation strain has a mean value ε_N and standard deviation s_N, and f_N is the volume fraction of the nucleated voids (see Chu and Needleman, 1980).

Table 2.
GTN damage parameters of 17vol.%SiCp/2009Al composite.

q_1	q_2	q_3	f_C	f_F	f_N	ε_N	s_N	r_0
1.5	1.0	2.25	0.03	0.045	0.04	0.3	0.05	0.9975

The presence of the first invariant of the stress tensor in the yield condition results in nondeviatoric plastic strains $\dot{\varepsilon}^{pl}$ and the plastic strains are derived from the yield potential:

$$\dot{\varepsilon}^{pl} = \dot{\lambda}\frac{\partial\phi}{\partial\sigma} \tag{19}$$

where $\dot{\lambda}$ is the nonnegative plastic flow multiplier, σ is the Cauchy stress tensor comprised of voids and the matrix material.

The evolution of $\bar{\varepsilon}^{pl}$ in the matrix material is obtained from the following equivalent plastic work expression:

$$(1-f)\sigma_y\dot{\bar{\varepsilon}}^{pl} = \sigma : \dot{\varepsilon}^{pl} \tag{20}$$

In the manufacturing process of the composite, the material cannot be fully dense so that the initial relative density of the porous material r_0 should be properly defined in the software. Besides, the integration of the elastoplastic equations for the GTN model is carried out using the backward Euler scheme proposed by Aravas (1987).

The material parameters of the 17vol.%SiCp/2009Al composite in the GTN damage model were determined based on the compression tests and are listed in Table 2. The thermo-physical properties of the composite used in the FE simulation are listed in Table 3 (Zhu and Kishawy, 2005). The work roll is assumed to be an analytical rigid surface, and only the heat capacity needs to be defined, which is assumed to be a constant of 460 J/(kg·°C) (Shahani et al., 2009) .

5. Results and discussion

5.1. Stress distributions

The distribution of stress components along the rolling, width and thickness directions at the steady state of model III are displayed in Fig. 7. From Fig. 7(a and b), it is clear that tensile stress appears at most of the contact area between the work roll and strip, and the highest tensile stress occurs at the edge of the strip and is perpendicular to the rolling direction. Meanwhile, in the width direction, the maximum

Table 3.
Thermo-physical properties of 17vol.%SiCp/2009Al composite (Zhu and Kishawy, 2005).

Young's modulus (GPa)	Poisson's ratio	Density (kg/m^3)	Thermal conductivity (W/(m·°C))	Coefficient of thermal expansion (1/°C)	Specific heat (J/(kg·°C))
101	0.34	2818	175	17.2×10^{-6}	900

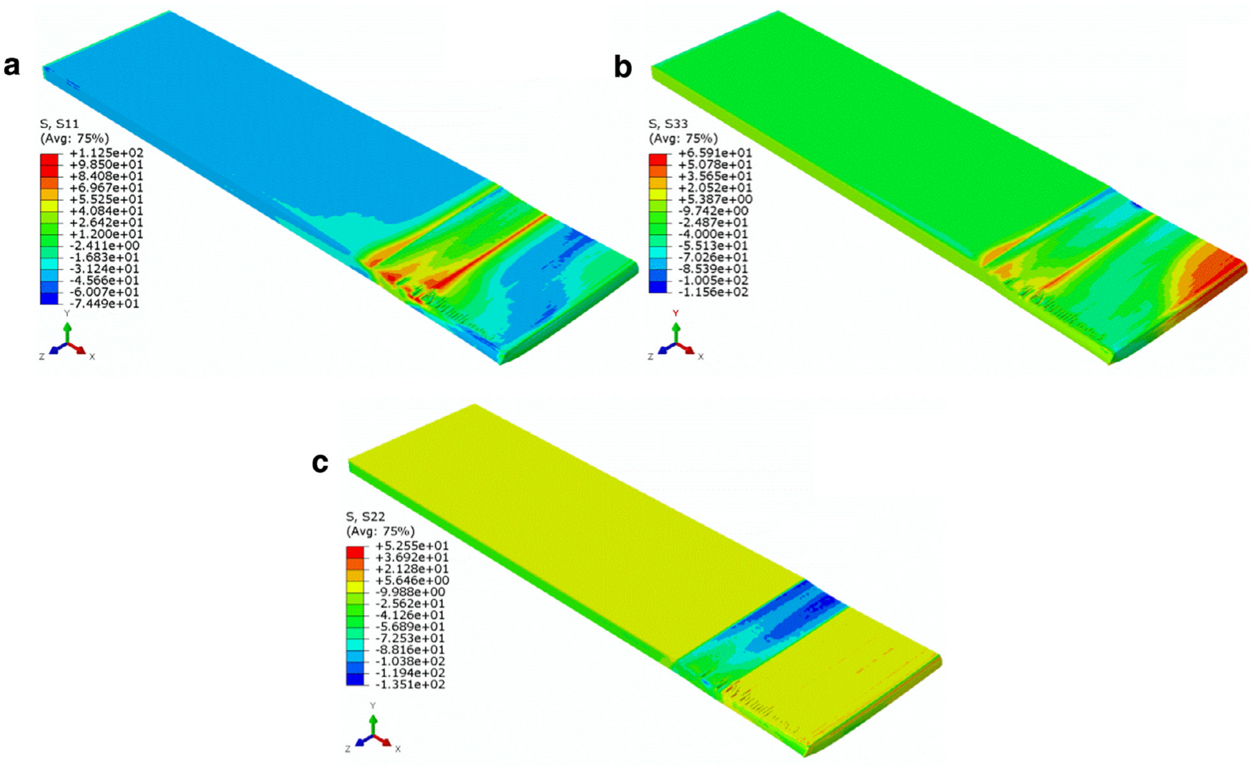

Fig. 7. Distributions of stress along (a) rolling, (b) width and (c) thickness directions.

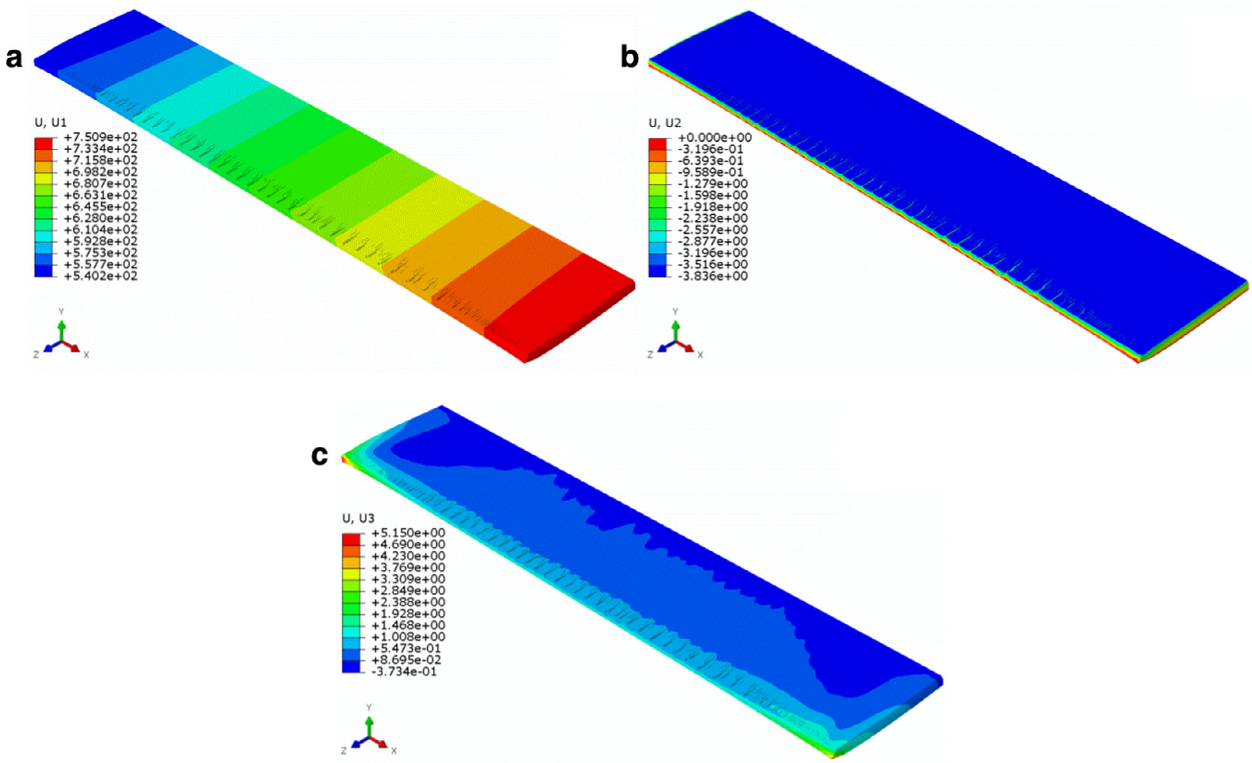

Fig. 8. Distributions of displacement along (a) rolling, (b) thickness and (c) width directions.

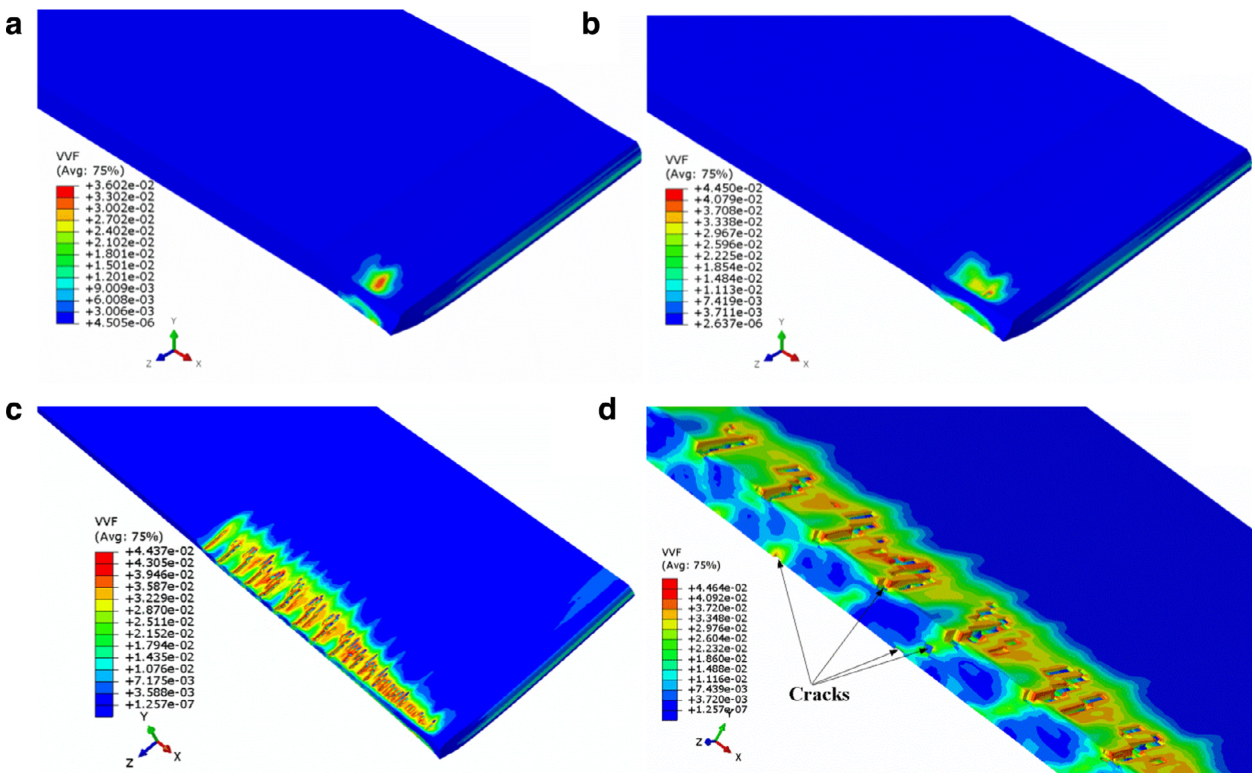

Fig. 9. Formation process of edge cracks during rolling of 17vol.%SiCp/2009Al composite.

tensile stress appears at the centre of the strip entrance, as shown in Fig. 7(b). In the thickness direction, the strip undergoes a higher compressive stress during the rolling process (Fig. 7c), and the compressive stress at the centre is higher than that at the edge. As is known, high tensile stress will contribute to crack initiation and propagation, while high compressive stress can prevent material from fracturing. Therefore, from the result of the stress distributions, it can be concluded that the initiation of cracks at the edge is easier than in other areas of the strip.

5.2. Displacement distributions

Fig. 8 shows the displacement distributions along the rolling, thickness and width directions of model III. From Fig. 8(a and b), it is clear that the deformation is uniform in the rolling process, and at a reduction of 30% (3.75 mm), the amount of longitudinal stretch is about 210 mm (see Fig. 8a). Fig. 8(c) shows the displacement field in the width direction. It can be seen that the displacement value of most of the edge of the strip is about 1 mm, and the maximum displacement value of 5.15 mm is concentrated at the outer edge of the strip exit.

The significant difference of displacement between the rolling and width directions can be explained by the law of minimum resistance. Since the contact length along the rolling direction is much smaller than that along the width direction and the contact shapes along the rolling and width directions are round and plane, respectively, the resistance along the rolling direction is lower than that along the width direction. Therefore, deformation along the rolling direction occurs much more easily than along the width direction. These results are consistent with the results of the stress distributions in Section 5.1; the highest stress of 112 MPa appears in the front of the contact zone along the rolling direction (Fig. 7a), while the lowest stress of about 35 MPa occurs at the outer edge of the contact zone along the width direction (Fig. 7b).

5.3. Formation process of edge cracks

Fig. 9 shows the evolution of damage and the formation process of edge cracks with the increase of rolling time. Fig. 9(a) shows the initial contact stage between the work roll and strip when the work roll approaches the strip and the maximum volume fraction of voids is concentrated at the edge of the strip. When the void volume fraction reaches the failure criteria, the element is removed and a crack appears, as shown in Fig. 9(b). As the void volume fraction accumulates continuously, more and more cracks initiate and propagate perpendicular to the rolling direction, as shown in Fig. 9(c). From these figures, it can be observed that the width

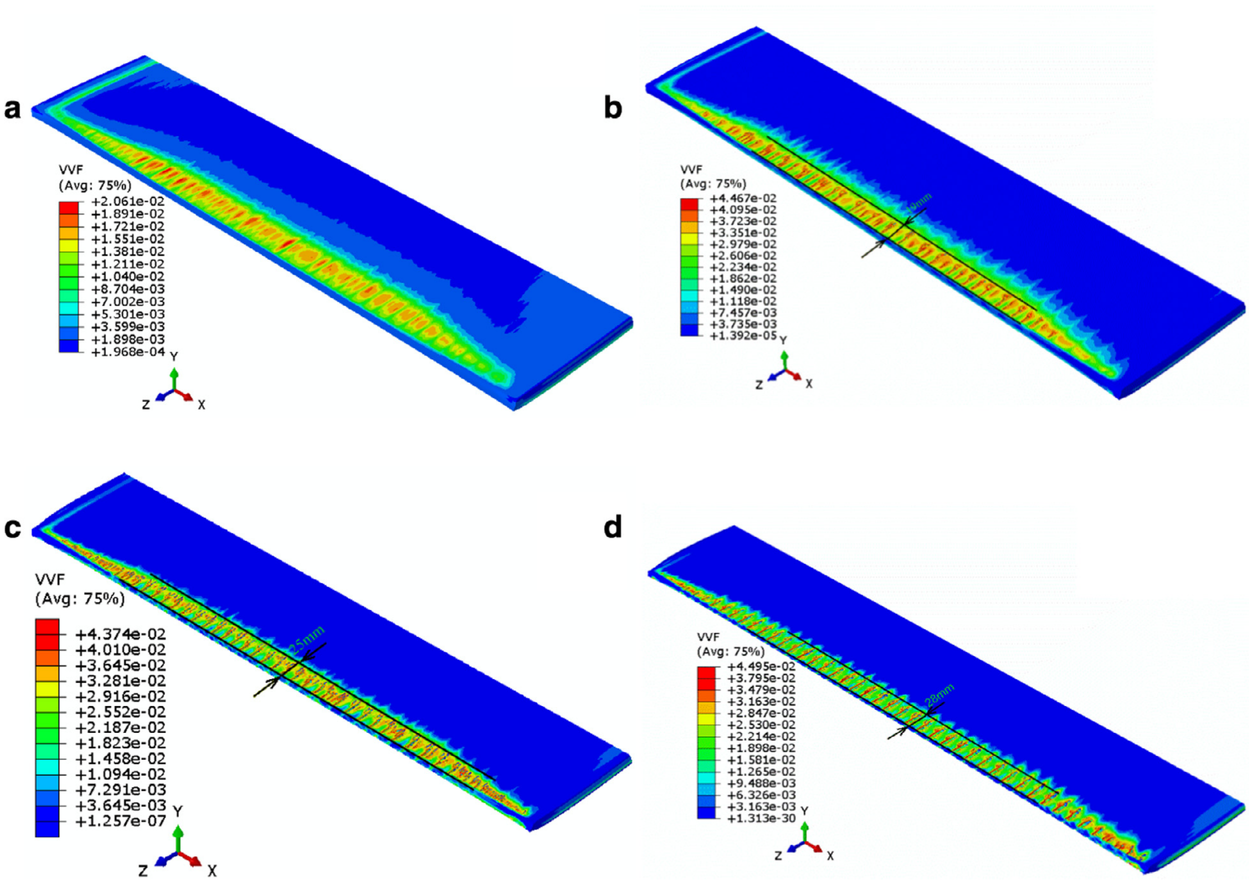

Fig. 10. Damage morphology of 17vol.%SiCp/2009Al composite on the strip at reduction of (a) 20%, (b) 25%, (c) 30%, and (d) 40%.

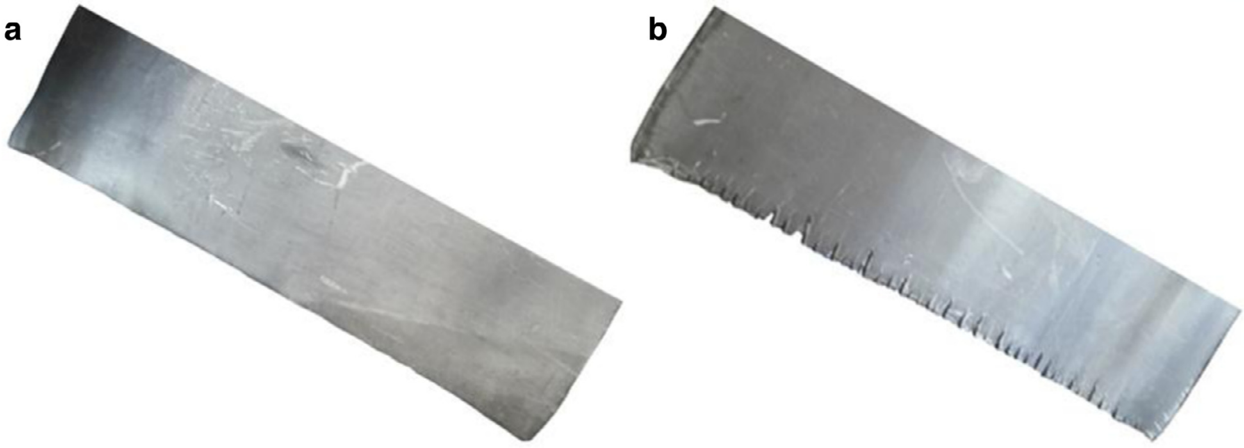

Fig. 11. Experimental results of edge morphology of 17vol.%SiCp/2009Al composite on the strip at reduction of (a) 20% and (b) 25%.

and spacing of the cracks increase gradually until the rolling reaches a steady state. In addition, a higher value of void volume fraction is also displayed at the centre of the strip entrance, which is consistent with the stress distribution along the width direction (Fig. 7b). Fig. 9(d) is the local amplified figure of Fig. 9(c), from which it is clear that there are also some small cracks occurring at the symmetry plane and the middle position of the model. Thus, with the increase of the total reduction, the edge cracks on the surface, symmetry plane and the middle region will connect and a deeper crack will appear or an edge fracture will occur, which may cause rupture of the strip in the rolling process.

5.4. Effect of the reduction

Since the reduction is one of the most important factors affecting the rolling process, rolling processes with different reductions are investigated. Fig. 10 shows the simulated edge damage morphology in rolling of the SiCp/2009Al composite under four different reductions. It is obvious that the edge damage is strongly influenced by the total reduction. At a reduction of 20%, no cracks occur and the damage is distributed on the surface (Fig. 10a). However, with the increase of the total reduction, the edge cracks initiate and propagate rapidly, and the width and depth increase gradually. When the total reduction increases from 25 to 40%, the length of the crack changes from 19 to 28 mm (Fig. 10(b and d)).

The edge morphology in hot rolled plates of 17vol.%SiCp/2009Al composite at reductions of 20 and 25% is shown in Fig. 11. It can be seen that there is no crack initiation at reduction of 20%, as shown in Fig. 11(a). With the reduction reached to 25%, plenty of cracks appear at the edge of the plate, as shown in Fig. 11(b). By comparing the simulated and experimental results, it is clear that the average length and spacing of cracks in the simulation are in good agreement with those in the experiment, and the damage morphology is also similar.

It is worth noting that the simulated crack distribution is more uniform than the experimental one. This can be explained by the present simulation model. In this model, the material is assumed to be homogeneous and the microstructure of the composite is not considered. In fact, besides many polyhedral SiC particles, the particle clusters and porosity in the composite could cause the uneven distribution of edge cracks. Hence, during hot rolling of the 17vol.%SiCp/2009Al composite, the total reduction should be less than 20% in one pass. Similar observations were reported in silicon steel (Yan et al., 2013) and SiCp/6061Al composites (El-Sabbagh et al., 2012) under different total reductions.

6. Conclusions

(1) The Arrhenius-type equations can be successfully used to model the flow behaviour of the 17vol.%SiCp/2009Al composite at elevated temperatures, and the influence of strain on the material parameters can be fitted by the fourth-order polynomial.
(2) During the rolling process, tensile stress occurs at the edge of the strip and is perpendicular to the rolling direction. On the contrary, compressive stress is displayed underneath the work roll along the thickness direction. This stress distribution results in the initiation and propagation of edge cracks perpendicular to the rolling direction.
(3) The total reduction has a significant influence on the edge damage. With increase of the total reduction, the width and depth of the edge cracks increase gradually. Therefore, a reduction of less than 20% in one pass should be selected in hot rolling of the 17vol.%SiCp/2009Al composite.

Acknowledgements

The authors gratefully acknowledge the support by the National Basic Research Program of China under grant no. 2012CB619600.

References

Abbasi-Bani, A., Zarei-Hanzaki, A., Pishbin, M.H., Haghdadi, N., 2014. A comparative study on the capability of Johnson-Cook and Arrhenius-type constitutive equations to describe the flow behavior of Mg–6Al–1Zn alloy. Mech. Mater. 71, 52–61.

Amirkhanlou, S., Rezaei, M.R., Niroumand, B., Toroghinejad, M.R., 2011. High-strength and highly-uniform composites produced by compocasting and cold rolling processes. Mater. Des. 32, 2085–2090.

Aravas, N., 1987. On the numerical integration of a class of pressure-dependent plasticity models. Int. J. Numer. Methods Eng. 24, 1395–1416.

Bagheripoor, M., Bisadi, H., 2011. Effects of rolling parameters on temperature distribution in the hot rolling of aluminum strips. Appl. Therm. Eng. 31, 1556–1565.

Balasubramanian, I., Maheswaran, R., 2015. Effect of inclusion of SiC particulates on the mechanical resistance behaviour of stir-cast AA6063/SiC composites. Mater. Des. 65, 511–520.

Chu, C.C., Needleman, A., 1980. Void nucleation effects in biaxially stretched sheets. J. Eng. Mater. Tech. 102, 249–256.

El-Sabbagh, A.M., Soliman, M., Taha, M.A., Palkowski, H., 2013. Effect of rolling and heat treatment on tensile behaviour of wrought Al-SiCp composites prepared by stir-casting. J. Mater. Process. Tech. 213, 1669–1681.

El-Sabbagh, A., Soliman, M., Taha, M., Palkowski, H., 2012. Hot rolling behaviour of stir-cast Al 6061 and Al 6082 alloys–SiC fine particulates reinforced composites. J. Mater. Process. Tech. 212, 497–508.

Esteban, L., Elizalde, M.R., Ocana, I., 2007. Mechanical characterization and finite element modelling of lateral spread in rolling of low carbon steels. J. Mater. Process. Tech. 183, 390–398.

Euh, K., Kang, S.B., 2005. Effect of rolling on the thermo-physical properties of SiCp/Al composites fabricated by plasma spraying. Mater. Sci. Eng. A 395, 47–52.

Gurson, A.L., 1977. Continuum theory of ductile rupture by void nucleation and growth: part I – yield criteria and flow rules for porous ductile media. J. Eng. Mater. Technol. 99, 2–15.

Hassani, A., Bagherpour, E., Qods, F., 2014. Influence of pores on workability of porous Al/SiC composites fabricated through powder metallurgy + mechanical alloying. J. Alloy. Compd. 591, 132–142.

Liu, J.W., Zheng, Z.X., Wang, J.M., Wu, Y.C., Tang, W.M., Lu, J., 2008. Pressureless infiltration of liquid aluminum alloy into SiC preforms to form near-net-shape SiC/Al composites. J. Alloy. Compd. 465, 239–243.

Lu, Y.X., Lee, C.S., Li, R.K.Y., Lai, J.K.L., 1999. The effect of cold rolling on the dynamic mechanical responses of SiCp/Al composites. J. Mater. Process. Tech. 91, 215–218.

Mansouri, L.Z., Chalal, H., Abed-Meraim, F., 2014. Ductility limit prediction using a GTN damage model coupled with localization bifurcation analysis. Mech. Mater. 76, 64–92.

Mei, R.B., Li, C.S., Liu, X.H, Han, B., 2010. Analysis of strip temperature in hot rolling process by finite element method. J. Iron. Steel. Res. Int. 17, 17–21.

Ni, D.R., Chen, D.L., Xiao, B.L., Wang, D., Ma, Z.Y., 2013. Residual stresses and high cycle fatigue properties of friction stir welded SiCp/AA2009 composites. Int. J. Fatigue 55 64–73.

Ni, D.R., Chen, D.L., Wang, D., Xiao, B.L., Ma, Z.Y., 2014. Tensile properties and strain-hardening behaviour of friction stir welded SiCp/AA2009 composite joints. Mater. Sci. Eng. A 608, 1–10.

Özdemir, Ì., Cöcen, Ü., Önel, K., 2000. The effect of forging on the properties of particulate-SiC-reinforced aluminum-alloy composites. Compos. Sci. Technol. 60, 411–419.

Pal, S., Ray, K.K., Mitra, R., 2010. Room temperature mechanical properties and tensile creep behavior of powder metallurgy processed and hot rolled Al and Al-SiCp composites. Mater. Sci. Eng. A 527, 6831–6837.

Sellars, C.M., McTegart, W.J., 1966. On the mechanism of hot deformation. Acta Metall 14, 1136–1138.

Seo, Y.H., Kang, C.G., 1999. Effects of hot extrusion through a curved die on the mechanical properties of SiCp/Al composites fabricated by melt-stirring. Compos. Sci. Technol. 59, 643–654.

Shahani, A.R., Setayeshi, S., Nodamaie, S.A., Asadi, M.A., Rezaie, S., 2009. Prediction of influence parameters on the hot rolling process using finite element method and neural network. J. Mater. Process. Tech. 209, 1920–1935.

Shao, J.C., Xiao, B.L., Wang, Q.Z., Ma, Z.Y., Liu, Y., Yang, K., 2010. Constitutive flow behavior and hot workability of powder metallurgy processed 20vol.%SiCp/2024Al composite. Mater. Sci. Eng. A 527, 7865–7872.

Tvergaard, V., Needleman, A., 1984. Analysis of the cup-cone fracture in a round tensile bar. Acta Metall 32, 157–169.

Yan, Y.X., Sun, Q., Chen, J.J., Pan, H.L., 2013. The initiation and propagation of edge cracks of silicon steel during tandem cold rolling process based on the Gurson–Tvergaard–Needleman damage model. J. Mater. Process. Tech. 213, 598–605.

Zhu, Y., Kishawy, H.A., 2005. Influence of alumina particles on the mechanics of machining metal matrix composites. Int. J. Mach. Tools Manuf. 45, 389–398.

Zhou, L., Wang, C.Z., Zhang, X.X., Xiao, B.L., Ma, Z.Y., 2015. Finite element simulation of hot rolling process for SiCp/Al composites. Acta Metall. Sin. 51, 889–896.